Journal of Materials Chemistry B

Albumin-polymer conjugate nanoparticles and their interactions with prostate cancer cells in 2D and 3D culture: degradable vs non-degradable polymers

Journal:	*Journal of Materials Chemistry B*
Manuscript ID	TB-ART-12-2015-002576.R1
Article Type:	Paper
Date Submitted by the Author:	17-Jan-2016
Complete List of Authors:	Jiang, Yanyan; University of new South Wales, Lu, Hongxu; University of New South Wales, Dag, Aydan; Bezmialem Vakif University, Hart-Smith, Gene; University of New South Wales, School of Biotechnology and Biomolecular Sciences Stenzel, Martina; University of New South Wales, School of Chemistry

Journal of Materials Chemistry B

ARTICLE

Albumin-polymer conjugate nanoparticles and their interactions with prostate cancer cells in 2D and 3D culture: comparison between PMMA and PCL

Received 00th January 20xx,
Accepted 00th January 20xx

DOI: 10.1039/x0xx00000x

www.rsc.org/

Yanyan Jiang,[a] Hongxu Lu,[a] Aydan Dag,[b] Gene Hart-Smith[c] and Martina H. Stenzel*[a]

Using proteins as the hydrophilic moiety can dramatically improve the biodegradability and biocompatibility of self-assembled amphiphilic nanoparticles in the field of nanomedicine. In this study, we fabricated and evaluated curcumin loaded albumin-polycaprolactone nanoparticles as a novel drug delivery system for prostate carcinoma therapeutics and compared their performance to poly(methyl methacrylate) (PMMA), a non-degradable and amorphous polymer. The maleimide functionalized poly(ε-caprolactone) (PCL) was obtain using ring opening polymerization (ROP) of ε-caprolactone where N-(2-hydroxyethyl)maleimide was used as an initiator. The resorbable albumin-polymer conjugate was prepared by conjugating the hydrophobic maleimide-terminated PCL to the hydrophilic bovine serum albumin (BSA) via a simple Michael addition reaction. PMMA was conjugated in a similar manner. The amphiphilic BSA-polymer conjugates can self-assemble into nanoparticles, displaying well-defined structure, prolonged storage stability, and excellent biocompatibility. The BSA nanoparticles, with encapsulated curcumin, exhibited highly enhanced antitumor activity compared to free curcumin. Furthermore, the high efficacy of the curcumin loaded nanoparticles was verified by effectively inhibiting the growth of three-dimensional LNCaP multicellular tumour spheroids. The cytotoxicity was attributed to the efficient cellular uptake of the nanoparticles through caveolic endocytosis. The direct comparison between PCL and the PMMA revealed that drug loading and release as well as cytotoxicity is not significantly affected by the nature of the polymer. However, it seems that nanoparticles based on PMMA penetrate quicker into LNCaP multicellular tumour spheroids thanks to the increased stability. The faster penetration was found to reduce the toxicity of the nanoparticles as evidenced by the lower number of dead cells. In contrast, the fully degradable PCL-based nanoparticles were more efficient in delivering the drug, thus limiting the growth of LNCaP multicellular tumour spheroids.

Introduction

Curcumin (diferuloylmethane) is a food chemical present in turmeric (Curcuma longa). It has been found to be pharmacologically safe as indicated by its consumption as a dietary spice for centuries.[1, 2] It possesses a wide range of pharmacological activities; for example, it possesses anti-amyloid, anti-oxidant and anti-inflammatory properties. Its usage has become increasingly attractive since it was found that curcumin has potent anti-proliferative and proapoptotic effects *in vitro* but low intrinsic toxicity.[3, 4] It has also been reported that curcumin could even suppress carcinogenesis in murine models.[5-7] Several lines of evidence strongly suggest that free curcumin induces cell cycle arrest and/or apoptosis and blocks nuclear factor kappa B (NF-κB) activation in various human cancer cell lines.[8] NF-κB is a ubiquitous transcription factor which controls the expression of various cytokines and the major histocompatibility complex gene.[9]

Prostate cancer, which is an aggressive, chemotherapy-resistant malignancy, is the most common cancer affecting males in developed countries and the second leading cause of cancer deaths in this group.[10, 11] The activation of NF-κB signaling in prostate cells increases osteoclastogenesis by up-regulating osteoclastogenic genes, thereby contributing to bone metastases formation.[12] Interleukin-6 (IL-6), an important NF-kB target gene, plays a critical role as a possible paracrine or autocrine growth factor for human prostate carcinoma cells.[10] Furthermore, NF-kB-regulated expression of genes such as interleukin-8 (IL-8), vascular endothelial growth factor (VEGF) and matrix metalloproteinase-9 (MMP-9) has also been found to be important for tumorigenicity, angiogenesis, and metastasis of prostate cancer cells.[13] Therefore, inhibition of NF-kB activity with curcumin, the compound that has been shown to target and inhibit activated NF-κB to restrict tumor cell growth in various cancer types, may offer an important new approach to the therapy of prostate cancer.

[a] Centre for Advanced Macromolecular Design (CAMD), School of Chemical Engineering and School of Chemistry, University of New South Wales, Sydney, NSW 2052, Australia; Email: M.Stenzel@unsw.edu.au
[b] Department of Pharmaceutical Chemistry, Faculty of Pharmacy, Bezmialem Vakif University, 34093 Fatih, Istanbul, Turkey
[c] Systems Biology Initiative, School of Biotechnology and Biomolecular Sciences, University of New South Wales, Sydney 2052, Australia

Electronic Supplementary Information (ESI) available: [NMR of initiator and polymer, GPC data of PCL, MALDI-TOF of polymer-protein conjugate, stability test of nanoparticles, details on inhibitors such as toxicity and concentrations used.]. See DOI: 10.1039/x0xx00000x

The efficacy of free curcumin for cancer therapy is limited by its poor solubility in water, which in turn limits its systemic bioavailability when administered orally.[9] The advances in nanoscale drug delivery vehicles, including polymeric micelles and liposomes, have resulted in greater control over the release and stability of therapeutic cargo. As an example, polymeric micelles, the core-shell structure fabricated by self-assembly of amphiphilic block copolymers with sizes of 20-100 nm, provide an effective strategy to transport hydrophobic drugs like curcumin.[14, 15] The hydrophilic corona enhances drug circulation time and the hydrophobic core serves as a reservoir of drugs.[16] Polymeric micelles ensure the preferential delivery of drugs to carcinoma sites owing to the enhanced permeability and retention (EPR) effect and certain smart design on the particle surface for targeting cellular uptake.[17, 18] However, concerns remain about the possible toxicities of some polymeric micelles that are not fully degradable and therefore might cause long-term effects. Inspired by the versatile properties of native proteins, hybrid drug carriers fabricated from proteins and synthetic polymers are increasingly described in literature.[19-23] In particular, albumin shows attractive features such as high biocompatibility and preferred lodgment in tumour sites.[24-26] The conjugation of polymers to albumin is now a widespread technique although the attachment of hydrophobic polymers, which results in the formation of giant hybrid amphiphiles, is less common.[19, 20, 27] The interest in giant amphiphiles stems from their self-assembly in aqueous media leading to the formation of micelles or other aggregates.[28] The resulting nanoparticles can be applied to deliver a variety of drugs ranging from hydrophobic anti-cancer drugs to genetic drugs.

Albumin is increasingly used as drug carriers. The drug is either conjugated to single albumin molecules or processed together with the drug to result in nano-sized albumin nanoparticles of sizes typically above 100 nm.[24, 29] Alternatively, albumin has been denatured and re-assembled together with a drug to generate monodisperse polymer carrier.[23, 30] Albumin as drug carrier is attractive due to not only the natural abundance in the body, but also its ability to interact with gp60 receptors and SPARC (Secreted Protein, Acidic and Rich in Cysteine), which are both overexpressed in cancers cells and tissue.[24, 31] Prerequisite for recognition by these receptors is the intact protein structure, which can easily be destroyed by extensive chemical modification.[32] The conjugation of polymers to Cys-34 on albumin is a well-known procedure that does not affect the activity of the protein.[19, 28, 33-35] Although this procedure was mainly carried out using water-soluble polymers, a considerable number of reports are available using hydrophobic polymers leading to giant protein amphiphiles, which can self-assemble resulting in micellar nanoparticles and other nanoparticles with protein shell.[19-2228] Inspired by easy access of protein coated nanoparticles by a simple self-assembly procedure, several polymers-albumin conjugates, among them conjugates based on PMMA,[31] PCL[36] and PDMAEMA,[35, 37] were tested in regards to their ability to encapsulate drugs.

The aim of this paper is to compare the effect of two different curcumin loaded albumin-coated nanoparticles which were prepared from PCL, a polymer that is semi-crystalline and resorbable and non-biodegradable PMMA polymers, respectively, in both 2D and 3D cell models. The PMMA or PCL nanoparticles resulted from self-assembly. In this paper, we compared the performance of both carriers in their ability to deliver curcumin to prostate cancer cell lines (PC3, DU145 and LNCaP) and to destroy LNCaP multicellular tumour spheroids.

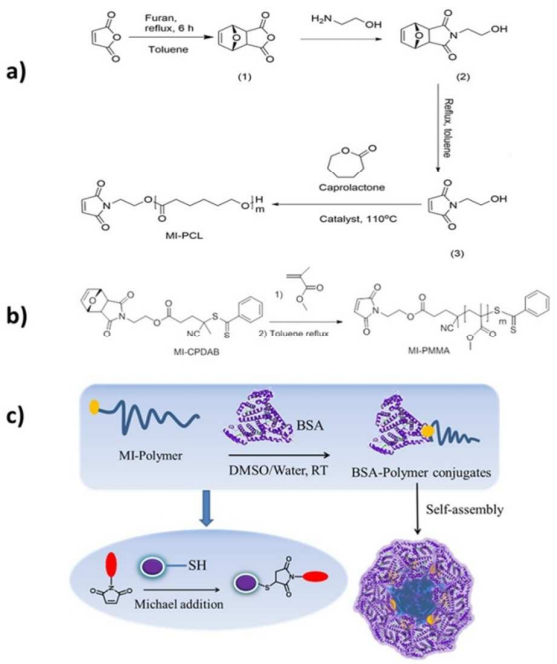

Scheme 1. Synthesis of protein-polymer conjugates based on PCL (a) or PMMA (b) and BSA and their self-assembly into nanoparticles (c)

Experimental

Materials

Unless otherwise specified, all chemicals were of reagent grade and used as received. Anhydrous methanol (Sigma-Aldrich, 99.8%), benzyl chloride (Aldrich, 99%), bovine serum albumin (BSA, Sigma, >96%), chloroform-D (CIL, 99.8%), curcumin (Sigma, >65% (HPLC)), dimethyl sulfoxide (DMSO, Ajax, 98%), ethanolamine (Ajax, 97%), furan (Aldrich, >99%), maleic anhydride (Fluka, >99%), sodium phosphate dibasic (Sigma-Aldrich, 98%), sodium phosphate monobasic (Sigma-Aldrich, >99%), sodium hydroxide (Aldrich, 98%), sodium chloride (Univar, reagent), 2,2',2'',2'''-(ethane-1,2-diyldinitrilo) tetraacetic acid (EDTA, Sigma-Aldrich, reagent), tetrahydrofuran (THF, Fisher Scientific, HPLC Grade, >99.9%), *N,N*-dimethylformamide (DMF, Ajax, 99.8 %) and toluene (Ajax, 99%) were used as received. ε-Caprolactone (ε-CL, 99%, Aldrich) was distilled from CaH_2 under vacuum. Methyl methacrylate (MMA, Aldrich, 99%, <30 ppm MEHG inhibitor) was purified by passing through a column of activated basic alumina to remove the inhibitor

The PMMA polymer was prepared according to a procedure described elsewhere.[31]

Synthesis of 4,10-Dioxatricyclo[5.2.1.0^{2,6}]dec-8-ene-3,5-dione (1) [38, 39]

Maleic anhydride (30.0 g, 0.3 mol) was suspended in 150 mL of toluene and the mixture warmed to 80 °C. Furan (33.4 mL, 0.45 mol) was added via syringe and the turbid solution was stirred for 8 h. The mixture was then cooled to ambient temperature and the white solids formed during standing were collected by filtration. The white solid was washed twice with petroleum ether (30 mL) and once with diethyl ether (50 mL), which afforded **1** as white needles. (Yield=44.4 g, 87%). ^{1}H NMR ($CDCl_3$) δ (ppm): 6.60 (s, 2H, C*H*=C*H*), 5.46 (s, 2H, -C*H*O, bridge-head protons), 3.21 (s, 2H, C*H*-C*H*, bridge protons). ^{13}C NMR ($CDCl_3$) δ (ppm): 169.8, 137.1, 82.2, 48.9.

Synthesis of 4-(2-hydroxyethyl)-10-oxa-4-azatricyclo[5.2.1.0^{2,6}]dec-8-ene-3,5- dione (2) [5, 40]

The adduct **1** (10.0 g, 60.0 mmol) was suspended in methanol (150 mL) and the mixture was cooled to 0 °C. A solution of ethanolamine (3.6 mL, 60 mmol) in 30 mL of methanol was added dropwise (10 min) to the reaction mixture and the resulted solution was stirred for 5 min at 0 °C and then 30 min at ambient temperature, followed by refluxing for 8 h. After cooling the mixture to ambient temperature, solvent was removed under reduced pressure, and residue was dissolved in 150 mL of CH_2Cl_2 and thrice washed with water (100 mL). The organic layer was separated, dried over Na_2SO_4 and filtered. Removal of the solvent under reduced pressure gave an almost colourless solid which was further purified by flash washing the product with ethyl acetate (EtOAc) to give the product as a white solid. (Yield=4.9 g, 40%). ^{1}H NMR ($CDCl_3$) δ (ppm): 6.55 (s, 2H, C*H*=C*H*), 5.23 (s, 2H, -C*H*O, bridge-head protons), 3.82-3.71 (m, 4H, NC*H*$_2$C*H*$_2$OH), 2.92 (s, 2H, C*H*-C*H*, bridge protons). ^{13}C NMR ($CDCl_3$) δ (ppm): 176.8, 136.5, 81.1, 60.4, 47.5, 41.8.

Synthesis of 1-(2-hydroxyethyl)-1*H*-pyrrole-2,5-dione (3) [5, 39]

4-(2-hydroxyethyl)-10-oxa-4-azatricyclo[5.2.1.02,6]dec-8-ene-3,5-dione (0.50 g, 2.39 mmol) was suspended in toluene (30 mL) and the solution was stirred at 110 °C overnight under nitrogen flow. The solution was evaporated under vacuum to afford the product as a white solid. (Yield= 0.33 g, 99 %). ^{1}H NMR ($CDCl_3$) δ (ppm): 6.76 (s, 2H, C*H*=C*H*), 3.85-3.70 (m, 4H, NC*H*$_2$C*H*$_2$OH), 2.05 (s, 1H, CH$_2$O*H*). ^{13}C NMR ($CDCl_3$) δ (ppm): 171.5, 134.7, 60.4, 40.4.

Preparation of maleimide functionalized PCL (MI-PCL)

MI-PCL was prepared by ring opening polymerization (ROP) of ε-CL (2.00 mL, 0.018 mol) in bulk using tin(II) 2-ethylhexanoate as a catalyst and **3** (0.025 g, 0.180 mmol) as an initiator at 110 °C for 3.5 h.[41] The following procedure was employed: to a previously flamed Schlenk tube equipped with a magnetic stirring bar, the degassed monomer, catalyst, and initiator were added in the order mentioned. The tube was degassed with three freeze–pump–thaw cycles and placed in a thermostated oil bath. After the polymerization, the mixture was diluted with THF and precipitated into an excess amount of cold methanol. The polymer was then isolated by filtration and dried at room temperature in a vacuum oven. The conversion was determined by ^{1}H NMR. ($M_{n,NMR}$=7560 g/mol; $M_{n,GPC}$= 7890 g/mol; M_w/M_n= 1.11; relative to PS standards) ^{1}H NMR ($CDCl_3$) δ (ppm): 6.75 (s, 2H, C*H*=C*H* of **3**), 4.28 (t, 2H, NCH$_2$C*H*$_2$OC=O of **3**), 4.19-3.96 (br, C*H*$_2$OC=O of PCL), 3.85-3.62 (m, C*H*$_2$OH of PCL end group and NC*H*$_2$CH$_2$OC=O of **3**), 2.38-2.22 (br, C=OC*H*$_2$ of PCL), 1.78-1.32 (m, C*H*$_2$C*H*$_2$C*H*$_2$ of PCL).

Preparation of the BSA-Polymer hybrid nanoparticle

Polymer (4 mg, 0.5 μmol) was dissolved in 3 mL of DMSO and a solution of bovine serum albumin (33 mg, 0.5 μmol) in 7 mL of PBS buffer (pH 7.4) was injected into the polymer solution under stirring. The mixture was stirred for 48 h and subsequently dialyzed against MilliQ water using a dialysis membrane (MWCO=6000-8000 Da). The supernatant containing BSA-PCL conjugate was finally collected and analyzed by MALDI-TOF, DLS and TEM.

Synthesis of the curcumin-loaded BSA-Polymer nanoparticle

Polymer (4 mg, 0.5 μmol) and curcumin (2 mg, 5.4 μmol) were dissolved in 3 mL of DMSO and then injected into the BSA solution (33 mg, 0.5 μmol) in 7 mL PBS buffer (pH 7.4) under stirring. The mixture was stirred for 48 h and subsequently dialyzed against water. The curcumin loaded BSA-PCL nanoparticle was collected and analysed by DLS and TEM. The curcumin encapsulation efficiency was analyzed using UV-Vis Spectroscopy. The Nile red loaded BSA-PCL nanoparticles and curcumin loaded BSA-PMMA nanoparticles were prepared *via* the same procedure.

Analysis Techniques

Nuclear Magnetic Resonance (NMR) Spectroscopy (^{1}H and ^{13}C NMR)

^{1}H and ^{13}C NMR spectra were recorded using a Bruker ACF300 (300 MHz) spectrometer, using $CDCl_3$ as the solvent. All chemical shifts were stated in ppm (δ) relative to tetramethylsilane (δ = 0 ppm), referenced to the chemical shifts of residual solvent resonances.

Dynamic Light Scattering (DLS)

The average hydrodynamic diameters and size distributions of aqueous nanoparticle solutions (1 mg/mL) were obtained using a Malvern Nano-ZS particle size analyzer (laser, 4 mW, λ=632 nm; measurement angle 12.8° and 175°). Samples were filtrated to remove dust using a microfilter 0.45 μm prior to the measurements and run for at least three times at 25 °C.

THF Gel Permeation Chromatography (THF GPC)

THF GPC was performed using a Shimadzu modular system containing a DGU-12A degasser, an LC-10AT pump, a SIL-10AD automatic injector, a CTO-10A column oven and a RID-10A refractive index detector. A 50×7.8 mm guard column and four 300×7.8 mm linear columns (500, 10^3, 10^4, 10^5 Å pore size, 5 μm particle size) were used for analyses. Tetrahydrofuran (THF, HPLC Grade) with a flow rate of 1 mL/min was used as the mobile phase. The injection volume was 50 μL. The samples were prepared by dissolving 2-3 mg/mL of the analyte in tetrahydrofuran, followed by filtration through a 0.45 μm filter. The unit was calibrated using

commercially available linear polystyrene standards (500-1000k Da, Polymer Laboratories). Chromatograms were processed using Cirrus 2.0 software (Polymer Laboratories).

Transmission Electron Microscopy (TEM)

TEM analyses were performed using a FEI Tecnai-G2 at 80-100 kV beam voltage. Samples were prepared by placing a droplet of solution on carbon-coated copper grids and draining the excess using filter paper. The dried samples were stained with uranyl acetate (3% aqueous solution) for 2 min.

Enzymatic Degradation

The enzymatic degradation of the BSA-PCL nanoparticles was carried out in two steps. Firstly, trypsin (in KH_2PO_4 buffer, pH 7.5) was employed to digest the albumin corona in 400 usp/mg protein working concentration. Thereafter, pancreatin (in KH_2PO_4 buffer, pH 7.5) was used to degrade the polyester core in 3X ups/mg protein working concentration. The samples were incubated in a test tube and shaken in a water bath at 37 °C. After the treatment of each enzyme, the test tubes were picked out and subjected to DLS analysis.

Mass spectrometry Analysis

Analyte solutions were prepared for MALDI analysis using 2,5-dihydroxybenzoic acid (DHB) (20 mg/mL in 70:30 acetonitrile:0.1% tetrafluoroacetic acid) as the matrix; samples were dissolved in 70:30 acetonitrile:0.1% tetrafluoroacetic acid (2 mg/mL). Matrix and sample solutions were mixed 1:1. 0.5 µL of this mixture was spotted on the sample plate, and the spots were dried in air at room temperature. MALDI mass spectra were recorded on a Bruker ultrafleXtreme MALDI–TOF/TOF spectrometer (Bruker, Bremen, Germany) using the following instrument parameters: accelerating potential = 25 kV, pulsed ion extraction = 450 ns, and laser frequency = 2000 Hz. The data from approximately 5000 shots were signal averaged to obtain a final spectrum. All data were processed using the Bruker flexAnalysis (version 3.4) software package.

Ultraviolet-Visible Spectroscopy (UV-Vis)

UV-Vis measurements were performed on a double beam VARIAN Cary 300 UV-Vis Spectrophotometer (PerkinElmer Differential Scanning Calorimeter) (<5 Abs, λ = 190-900 nm) over the visible range (λ = 400-800 nm) at 25 °C. Samples containing curcumin were dissolved in *N,N*-dimethylformamide (DMF) and measured in a quartz cell with a path length of 10 mm to obtain the calibration curve. A calibration curve was created testing the absorbance of a range of concentrations of curcumin dissolved in DMF (0.095–16.2 µM) through the UV-Vis Spectroscopy (λ = 420 nm) and the curcumin encapsulation efficiency was analyzed with the results compared to this calibration curve.

Measurement of Drug Release Rate from Protein-Polymer conjugated nanoparticles

5 mL of the polymer-protein curcumin carrying nanoparticle solution was dialysed in 200 mL of PBS buffer (pH=7.4) at 37 °C. Aliquots of the samples which were taken out from the membrane tube at different time points over the period of 96 hours were then freeze dried and redissolved in DMF. The samples were then analysed *via* UV-Vis spectrometry and their absorbance was compared to the calibration curve.

Cytotoxicity testing

Human prostate carcinoma PC3, DU145, and LNCaP cells were cultured in tissue culture flasks with Medium RPMI1640 supplemented with 10% fetal bovine serum at 37 °C under a 5% CO_2 atmosphere. After reaching confluency, cells were collected from the flasks with Trypsin/EDTA treatment. The cell suspension was then seeded into a 96-well cell culture plate at a cell density of 30,000 cells/mL and 100 µL/well. After incubation for 1 day, the cells in the plate were subsequently used for cytotoxicity test. This involved sterilizing the nanoparticles by UV irradiation for 20 min and serially diluting by half the solution with sterile water. The old medium in the cell culture plate was discarded and replaced with 100 µL of fresh twice-concentrated RPMI1640 medium and the cells were incubated with the nanoparticles for 48 h. The cell was then fixed by the addition of cold TCA. The culture medium was discarded and 100 µL of 10% TCA was added to each well, followed by incubation of the plates for 30 min at 4 °C. The supernatant was discarded and the plates washed 5 times with water and air-dried. 100 µL of SRB solution 0.4% (w/v) in 1% acetic acid was added to each well, and the plates incubated for 15 min at room temperature. After staining, the unbound dye was removed by washing 5 times with 1% acetic acid and air-dried. Bound stains were dissolved with 200 µL 10 mM Tris Buffer and absorbance was measured on a Bio-Rad BenchMark microplate reader (λ = 490 nm). The data was analyzed and plotted using GraphPad Prism 6.0.

Prostate multicellular tumour spheroid (MCTS) preparation and drug treatment

The cell density of LNCaP cell suspension was adjusted to 100,000 cells/mL. 10 µL of the cell suspension was gently dropped onto the lid of the 100 mm cell culture dish. The lid was then slowly turned over and placed onto the dish which was filled with 20 mL sterile PBS to maintain the humidity of the inner dish chamber. The cells were incubated and kept undisturbed at 37 °C at 5 % CO_2 for 7 days. The MCTS were transferred to a 96-well U-bottom suspension culture plate (Corning) and cultured for 1 day before further experiments. Sterile MilliQ water (as a control), free curcumin and the curcumin loaded BSA-PCL nanoparticles were added to the spheroids. The curcumin concentration of both the free curcumin and the nanoparticle in each culture well was 0.15 mM. The morphology of the MCTS after 0 day and 7 days was recorded using a Leica DM IL inverted microscope equipped with a ProgRes® Scan camera (Warner Instruments, LLC) and the sizes were analysed using the software ProgRes® CapturePro. For the comparison between BSA-PCL nanoparticle and BSA-PMMA nanoparticle, the similar protocol was used except that the concentration of the curcumin in both the two nanoparticles was 30 µM.

Quantification of DNA amount in each spheroid.

Three pancreatic spheroids in each sample group were collected into a 1.5 mL centrifuge tube, washed with PBS thrice and rinsed

with MilliQ water. The spheroids were lyophilized and dispersed in 100 µL lysis buffers (0.5% sodium dodecyl sulfate (SDS) in 50 mM Tris, pH 8.0) and incubated overnight at 4 °C to completely dissolve the DNA in the spheroid into the lysis buffer. An aliquot of lysate was used to measure the DNA content of spheroids with Hoechst 33258 based DNA Quantitation Kit (Sigma-Aldrich) under a Cary Eclipse Fluorescence Spectrophotometer (Agilent Technologies) at excitation = 360 nm and emission = 460 nm. The fluorescence values were used to calculate cell numbers based on a standard curve made from the standard DNA provided with the kit.

Cellular uptake observed using laser scanning confocal microscopy

LNCaP cells were seeded in 35 mm Fluorodish (World Precision Instruments) at a density of 100,000 cells per dish and cultured for 3 days with the RPMI1640 medium supplemented with 10% fetal bovine serum. Nanoparticle solutions were loaded to LNCaP cells at a working concentration of 50 µg/mL and incubated at 37 °C for 2 h. After incubation, the cells were washed thrice with PBS (pH 7.4). The cells were then stained with Hoechst 33342 for 10 min followed by staining with 100 nM LysoTracker Red DND-99 (Invitrogen) for 1 min. The dye solution was quickly removed and the cells were gently washed with PBS. Finally, the cells were mounted in PBS and observed under a laser scanning confocal microscope system (Zeiss LSM 780). The system was equipped with a Diode 405-30 laser, an argon laser and a DPSS 561-10 laser (excitation and absorbance wavelengths: 405 nm, 488 nm and 561 nm, respectively) connected to a Zeiss Axio Observer. The ZEN2011 imaging software (Zeiss) was used for image acquisition and processing.

Cellular uptake efficiency analyzed by flow cytometry

LNCaP cells were seeded in 6-well cell culture plate at a density of 500,000 cells/well and incubated at 37 °C with 5 % CO_2 for 1 day prior to nanoparticle treatment. During treatment, the medium was replaced with the RPMI1640 cell culture medium containing nanoparticles (40 µg/mL working concentration) at 37 °C and incubated for 2 h. The cell monolayer was washed 3 times with cold PBS and treated with trypsin/EDTA. The cells were collected, centrifuged and resuspended in cold serum free culture medium. The cell suspensions were used for flow cytometry analysis on BD FACSCanto™ II Analyser (BD Biosciences, San Jose, USA), collecting results from at least 50,000 events.

Endocytosis inhibitor treatment

LNCaP cells were seeded in 24-well cell culture plates at a density of 100,000 cells per well and incubated at 37 °C with 5 % CO_2 for 1 day prior to nanoparticle treatment. The 24-well plate was pre-incubated for 30 min at 37 °C with various endocytosis inhibitors: chlopromazine (10 µg/mL), filipin (20 µg/mL), amiloride (50 µM) and NaN_3 + deoxyglucose (5 mM+10 mM) solution. Those inhibitors showed no toxicity to the cells (**ESI, Figure S13**). The old medium with inhibitors was discarded and replaced with 400 µL fresh RPMI1640 medium and 100 µL FITC-labeled nanoparticle solution, followed by incubating for 1 h at 37 °C in 5% CO_2. The cell monolayers were washed 3 times with 500 µL cold PBS. The amount of the internalized nanoparticles was quantified by measuring the fluorescence intensity of the nanoparticle solution together with the washing PBS using a Cary Eclipse Fluorescence Spectrophotometer (Agilent Technologies) at λ_{ex} = 490 nm and λ_{em} = 512 nm. The values were then compared to the fluorescence intensity of the solution at t=0 min. The experiments were carried out in quadruplicate. The same experiment was carried out for 24 h.

Results and discussion

Preparation of curcumin loaded BSA-PMMA nanoparticles

The synthesis and conjugation of MI-PMMA and the conjugation to BSA was discussed in detail in an earlier publication.[31] The polymer (M_n= 9,000 g/mol) was conjugated to BSA in a mixture of DMSO and PBS buffer in the presence of curcumin. The curcumin loading efficiency of the resulting nanoparticles (D_h= 147 nm, ξ= -30.1 mV) **(Figure S1)** was found to be 63% while the drug encapsulation capacity was 31.5 %

Preparation of curcumin loaded BSA-PCL nanoparticles

The initiator for the polymerization of ε-CL was prepared within three steps as shown in **Scheme 1**. In the first step, furan and maleic anhydride were reacted in toluene at 80 °C for 8 h. The obtained product **1** was utilized for the synthesis of **2** by adding a solution of 2-amino ethanol in methanol into the dispersion of **1** in methanol. Finally, **3** was obtained by refluxing **2** in toluene, which led to the deprotection of the furan-functionality in a retro Diels-Alder reaction (**ESI**, **Figure S2-S7**). Subsequently, **3** was employed for the ROP of ε-CL in bulk. The polymer was obtained with high maleimide end group fidelity that was characterized with ^{1}H NMR (**ESI, Figure S8a**). The molecular weight $M_{n,GPC}$ of MI-PCL was determined to be 8000 g/mol based on linear PS standards (**ESI, Figure S8b**), which is in good agreement with the molecular weight calculated from NMR by comparing the methylene signal adjacent to the ester at 4.1 ppm with the endfunctionality at 6.75 ppm. MALDI-TOF analysis was consistent with these data (**ESI, Figure S9**), as discussed below.

Following the purification of MI-PCL, the polymer with maleimide end group was dissolved in DMSO and then mixed with the BSA solution in PBS buffer. The final mixture was left to stir for 48 h to achieve maximum yield of the Michael addition reaction between the thiol group on BSA and the maleimide group at the end of the MI-PCL polymer chain. Thereafter, micellization of the BSA-PCL conjugate took place during dialysis against water. It should be noted here that the resulting core-shell nanoparticles are not micelles in the traditional sense, but rather nano-precipitated aggregates with an albumin surface layer. DLS analysis was employed to determine the hydrodynamic diameter and the size distribution of the blank BSA-PCL nanoparticles after dialysis. The size distribution is depicted in **Figure 1a** revealing an average hydrodynamic diameter of the BSA-PCL nanoparticle of around 100 nm and a PdI of 0.2, which is significantly smaller that the curcumin loaded 225 nm nanoparticles prepared by the desolvation process in the absence of polymer.[42] TEM analysis (**Figure 1b**) confirmed that nanoparticles were obtained with spherical morphology. The

particle size measured by TEM was in good agreement with that of DLS considering the dried state of the nanoparticles under TEM analysis which led to dehydration.

The stability of the BSA-PCL nanoparticles was investigated by characterizing the particle size and shape of the nanoparticle stored at 4 ^{o}C. As shown in **Figure 1** and **ESI, Table S1**, the morphology of the nanoparticles after 5 days was close to that of the fresh sample, suggesting that the BSA-PCL nanoparticles can be conserved for an extended period of time. Although this albumin based drug carrier is stable in aqueous solution, it can quickly degrade in the presence of enzymes. Enzymes can therefore help to elucidate the structure of the nanoparticle. Trypsin, a serine protease that hydrolyses proteins, was observed to deplete the albumin corona. The remaining hydrophobic PCL started to aggregate after a couple of minutes and precipitate, which was confirmed by the increase of the measured hydrodynamic diameter **(Figure 1a** and **Table S1)**. The quick degradation can therefore confirm that albumin is indeed enriched on the surface. Subsequently, pancreatin, which is a mixture of amylase, lipase and protease, was added to allow digestion of the ester bond of PCL. After 5 min, the solution turned clear and dissolved the precipitated PCL, which led to the absence of any detected nanoparticles in DLS. It should be noted here that the addition of enzymes should only confirm the presence of degradable functionalities and will not indicate the degradation occurring *in vitro* or *in vivo*. In fact, PCL is known to undergo only very slow degradation in vivo lasting several months. However, it is still an attractive material for drug delivery purposes as it has been shown to be resorbable over time.[43]

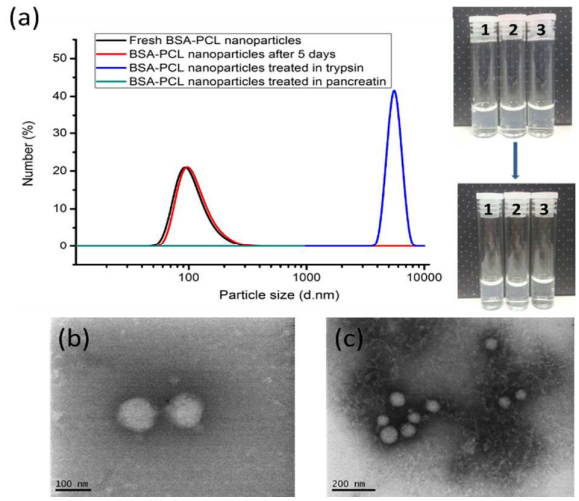

Figure 1. (a) Sizes of the blank BSA-PCL nanoparticles before and after enzymatic digestion for 5 min. The inset is the corresponding appearance of samples before and after enzymatic digestion. Sample 1 is the control without enzyme added; sample 2 is the sample degraded with trypsin; and sample 3 is the sample digested by pancreatin. (b) TEM image of the fresh BSA-PCL nanoparticles; (c) TEM image of the BSA-PCL nanoparticles after 5 days.

The conjugation between BSA and PCL was confirmed using MALDI-TOF analysis. The MALDI-TOF spectrum of the polymer was dominated by peaks corresponding to sodium adducts of the expected MI-PCL product (**ESI, Figure S8**); given that mass-based ionization bias effects are likely to be operative during the MALDI process, the observed M_n of ~7300 g/mol for the polymer is in agreement with the M_n data obtained *via* NMR and GPC. The molecular weight of native BSA was measured as ~66K g/mol (*m/z*=~33K for the doubly-charged BSA and *m/z*=~133K for the BSA dimer), as shown in the top spectrum in **ESI, Figure S10**. The MALDI-TOF spectrum of the conjugate sample (bottom spectrum in **ESI Figure S10**) confirmed the successful PCL and BSA conjugation, as indicated by the peaks observed at *m/z*=~74K (singly-charged BSA and PCL conjugate), *m/z*=~37K (doubly-charged BSA and PCL conjugate), and *m/z*=~141K (singly-charged BSA dimer and PCL conjugate). In addition, these peaks indicated that the conjugation approach resulted in one-to-one reaction. Based on the results from the SDS-PAGE image, equimolar amount of albumin and PCL led to a conjugation efficiency of about 50%. (**ESI, Figure S11**)

Similar to the loading of curcumin into PMMA-based albumin nanoparticle, the drug was dissolved together with MI-PCL prior to the addition of albumin. Mixing the organic polymer-drug phase and the aqueous albumin solution triggers several simultaneous processes: polymer-protein conjugation, self-assembly into micellar particles and curcumin encapsulation into the PCL cores of the nanoparticles. DLS analysis (the black curve in **Figure 2a**) and the TEM image (**Figure 2b**) of the curcumin loaded BSA-PCL nanoparticles revealed a particle size of 125 nm with a narrow distribution and a clearly-defined spherical structure. Subsequently, the nanoparticle sample was analyzed *via* UV-Vis spectrometry which gave a drug loading efficiency of around 54% and a drug encapsulation capacity of 27%. Around half of the loaded curcumin was released after 24 hours and reached more than 80% after 50 h.

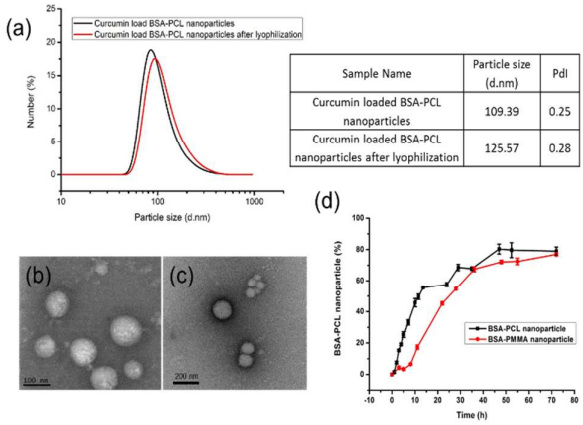

Figure 2. Characterization of the curcumin loaded nanoparticles (a) DLS analysis before and after freeze drying (b) TEM analysis before and (c) after freeze-drying; (d) release of curcumin.

The prepared particles show high drug loading, high stability in solution and display the desired degradability. Another crucial parameter is the storage of the loaded nanoparticles. Drug formulations are often stored in solid form to extend product shelf life. A prerequisite for storage in the solid form is easy dissolution into aqueous media by applying a simple vortex process with or without mild heating.[44] The most common method for preparing solid protein pharmaceuticals is lyophilization.[45] Therefore, the

curcumin loaded BSA-PCL nanoparticle solution was lyophilized, followed by resuspension. As is evident from the TEM and DLS analyses (**Figure 2**), the freeze-dried nanoparticles could be completely dissolved without any visible size changes or loss of structure. The products could therefore be stored as a yellow powder for an extended period of time.

According to the aforementioned characterization, we have generated two nanoparticles, based on PMMA and PCL respectively, with similar properties, e.g. particle size, drug loading efficiency, etc. (**Figure 2** and **ESI, Figure S1**) As listed in **Figure 2d**, the release of curcumin seems slightly accelerated in the BSA-PCL nanoparticles, but crucial is that after 48 hours, the time point for the following cytotoxicity test, 80% of the drug has been released from both nanoparticles. It can safely be assumed that these values are accelerated inside the cell considering the large amount of enzymes that will cause degradation. In the following, the activity of both the two curcumin loaded nanoparticles will be investigated to evaluate the effect of degradation of the polymer on performance.

Cell uptake

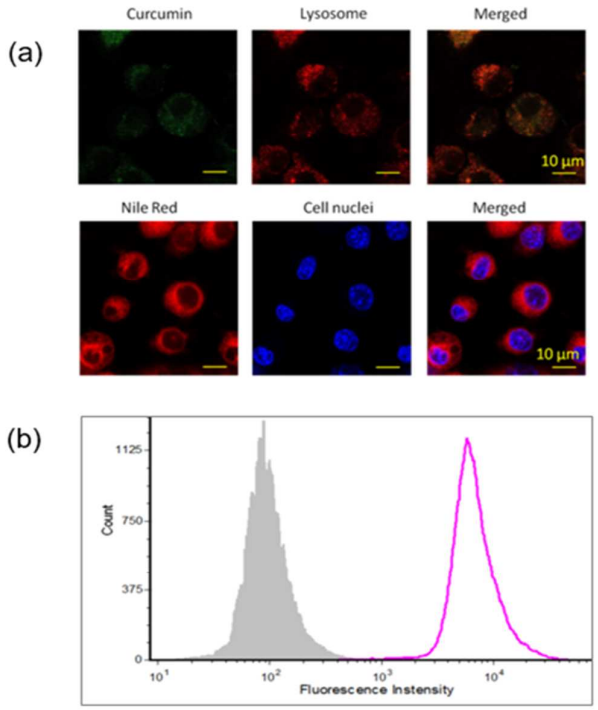

Figure 3. (a) Confocal microphotographs of LNCaP cells after incubation with nanoparticles at 37 ^{o}C for 2 h. Nanoparticles were loaded with curcumin (green, top) and Nile red (red, bottom). Lysosomes (Red) were stained with LysoTracker Red DND-99. Cell nuclei (blue) were stained with Hoechst 33342. Scale bar is 10 µm. (b) Flow cytometry analysis of Nile red labelled BSA-PCL nanoparticle (pink curve) uptaking into LNCaP carcinoma cells after 2 h. The grey area is the control.

Prior to cell viability studies the cellular uptake was investigated in detail. There is strong evidence that albumin transcytoses into cells *via* the gp60 receptor,[46, 47] an endothelial cell membrane 60-kDa albumin-binding protein localized in caveolae. Today, a range of other cellular albumin binding proteins and receptors have been identified.[48] To understand the cellular uptake of this drug carrier in more detail, flow cytometry in combination with various uptake inhibitors was employed. Prior to this, the uptake was monitored using confocal fluorescent microscopy (**Figure 3a)** using LNCaP cells. The cells were incubated for 2 h with either curcumin loaded BSA nanoparticles (top) or Nile red loaded nanoparticles (**ESI, Figure S12**) as non-toxic alternative (bottom). The cells were in addition stained to highlight the lysosomes (LysoTracker DND-99) in curcumin loaded BSA nanoparticle treatment and the cell nuclei (Hoechst 33342) in Nile red loaded nanoparticle treatment, respectively. The drug-loaded nanoparticles in the cells exhibited either green (curcumin) or red (Nile red) fluorescence dependent upon the emission wavelength. After incubation with the LNCaP cells for 2 h, the BSA nanoparticles underwent rapid internalization and accumulation by the cancer cells. According to the confocal microscopy images, these nanoparticles were located in the lysosomes (red). In images for the Nile red loaded nanoparticles, cytosols and cytoskeleton were also stained which indicates the release of Nile red from the nanoparticles. To further quantify the uptake process, the internalization of the albumin nanoparticles into LNCaP cells was analysed *via* flow cytometry using by measuring fluorescence intensity of the Nile red labelled BSA-PCL nanoparticles (**Figure 3b**). After 2 h, a large proportion (approximate 97%) of cells was found to internalize the albumin nanoparticles.

The amount of the internalized nanoparticles could be determined by monitoring the fluorescent intensity of the solution used for cell incubation. Upon cell uptake of fluorescent nanoparticles into LNCaP, the fluorescent intensity of the solution declines.[49] Added endocytosis inhibitors provide subsequent information on the type of uptake including clathrin-mediated endocytosis, caveolae-mediated endocytosis, clathrin- and caveolae-independent endocytosis, phagocytosis, and macropinocytosis.[50, 51] Herein, sodium azide plus deoxyglucose (NaN_3+DG), chlopromazine (CPZ), filipin, and amiloride were used to inhibit the energy-dependent endocytosis, clatherin-mediated, caveolae-mediated, and macropinocytosis, respectively. It was demonstrated that none of the inhibitors had an effect on the cell growth (**ESI, Figure S13a**). Except the CPZ inhibitor, all the other inhibitors also had no evident effect on the fluorescence intensity (**Figure 12b**). The function and the dosage of the inhibitors have been listed in **ESI, Table S2** and **Table S3**. As shown in **Figure 4a**, about 10% of FITC-labeled BSA-PCL nanoparticles were taken by the LNCaP cells. When treated with filipin and NaN_3+DG, the amount of internalized nanoparticles decreased compared to the other two inhibitors and the control. It is indicated that filipin and NaN_3+DG hampered the uptake of the BSA-PCL nanoparticles. Although the inhibitory effect of NaN_3+DG was higher than that of filipin, there was no statistical difference between those two inhibitors. As for NaN_3+DG, it works by completely blocking energy-dependent endocytosis through ATP depletion. Filipin showed very profound effects in preventing the internalization of the nanoparticles, which was valid evidence that uptake of these nanoparticles is predominantly caveolic. The inhibitory effects were also confirmed with longer 24 h incubations

(**Figure 4b**). As gp60 receptors trigger caveolae endocytosis via a Gi-coupled src kinase–mediated pathway,[52] the specific binding between BSA-PCL nanoparticles and gp60 receptors may play an important role in the caveolae-mediated endocytosis. Both nanoparticles lead to similar results since the uptake is only dependent on the type of the shell and the size.

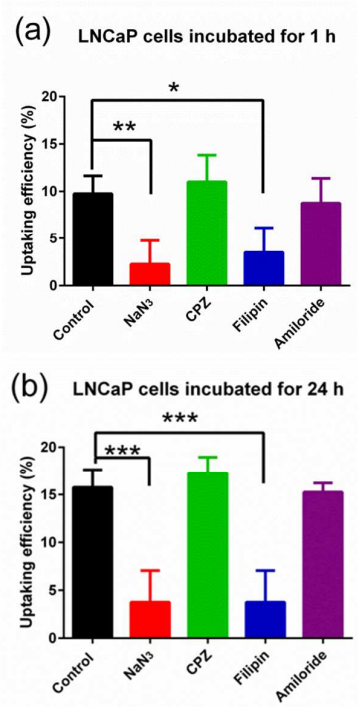

Figure 4. Inhibition assays of LNCaP cells against four inhibitors: CPZ, filipin, amiloride and NaN_3+DG. (a) LNCaP cells against the four inhibitors for 1 h. (b) LNCaP cells against the four inhibitors for 24 h. Data represent means ± S.D., n=4. *, statistical difference, p< 0.05. **, statistical difference, p< 0.01. ***, statistical difference, p<0.001.

In vitro cytotoxicity test

The toxicity of both curcumin loaded nanoparticles (PMMA and PCL) was determined after 48 h incubation at 37 °C using the prostate cancer cell line LNCaP. Prior to this study, the toxicity of curcumin alone was evaluated (**ESI, Figure S14 a** and **Figure 5**). Previous studies[53] showed the IC50 (the concentration at 50% cell death) of free curcumin is in a range of 10 to 25 µM against different cell lines (Human leukemia (KBM-5 and Jurkat), breast (MDA-MB-231), colon (HCT116) and esophageal (SEG-1) cancer cells). However, the measured IC50 value of free curcumin against various prostate cancer lines (PC3, DU145 and LNCaP) is well above these values (> 27 µM) (**ESI, Figure S14 a**). Curcumin can therefore be deemed non-toxic in the concentration range measured. As the blank BSA-PCL **(ESI, Figure S14 b)** and BSA-PMMA[31] nanoparticles showed no toxicity, the evident reduction in the IC50 value with the curcumin loaded nanoparticles should be attributed to the enhanced uptake of curcumin using the nanoparticle as a shuttle (**Figure 5**). To confirm that this significantly enhanced toxicity of curcumin by using a BSA-based drug carrier is not unique to LNCaP, other prostate cancer cell lines such as PC3 and DU145 were tested revealing similar results (**ESI, Figure S14c**). The toxicity of both nanoparticles was found to be within similar range (**Figure 5**). Considering that both nanoparticles have comparable physico-chemical features including a high drug release after 48 h the similarity in toxicity may not be surprising.

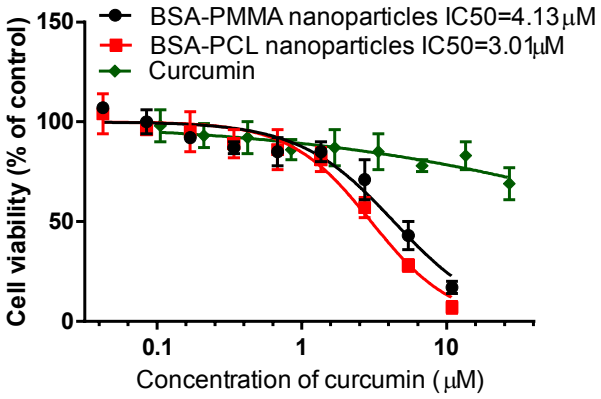

Figure 5. Cytotoxicity assays of curcumin alone and curcumin loaded BSA-PCL and BSA-PMMA nanoparticles against prostate carcinoma cell lines LNCaP for 48 h. The mean±standard deviations are shown.

So far, the differences between both nanoparticles are not obvious. This is not surprising since the assays employed use condition where degradation and stability does not play a major role. The uptake of both nanoparticles is fast and there does not seem to be a difference if the drug is liberated from the nanoparticles by leaching from the carrier or by degradation over the next 48 hours. Both nanoparticles show similar rates of release. Analysis of nanoparticles in multicellular tumour spheroids, which can be considered closer to real tissue in terms of cell metabolism and gene profiles,[54] can in contrast be more sensitive to these differences as the nanoparticles now penetrate into the spheroid by a series of endo- and exocytosis events. Nanoparticles of higher stability were shown to diffuse at a faster rate,[55, 56] probably because of an accelerated rate of exocytosis.

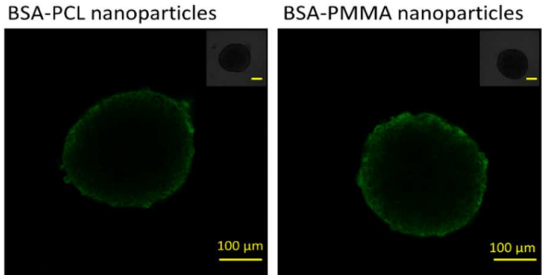

Figure 6. Confocal fluorescent microscope images of prostate carcinoma LNCaP spheroids treated with BSA-PCL nanoparticles

(left) and BSA-PMMA nanoparticles (right) for three hours. Both nanoparticles were labelled with equivalent amounts of curcumin.

After 3 hours the higher rate of penetration of BSA-PMMA nanoparticles is visible (**Figure 6**). Since it can be assumed the PCL is not degraded after 3 hours due to its high resistance to degradation,[43] and most physico-chemical parameters are similar in both nanoparticle, the origin of the slightly faster penetration is unknown.

Faster penetration does not necessarily translate into higher toxicity as the nanoparticles need to reside within the cell sufficiently enough to be able to unload their toxic cargo. The LNCaP spheroids were incubated with a low curcumin concentration of 30 µM to ensure that the differences between the two nanoparticles are visible. Higher concentrations of drug can be too effective in destroying the spheroids, which does not allow identifying the more efficient nanoparticle. Analysis of the viability of the LNCaP spheroid after 7 days' incubation reveals that the BSA-PCL nanoparticles were more successful in inhibiting growth of the spheroids (**Figure 7**). It therefore seems that a high rate of penetration is not prerequisite for the efficient delivery, but rather a well-matched rate of transport and rate of drug release.

To evaluate the ability of the drug carrier to fully inhibit the growth of the spheroid, a drug concentration of 150 µM was employed. The LNCaP spheroids were now incubated with MilliQ water (control), free curcumin and curcumin loaded BSA nanoparticles for 7 days at 37 °C, respectively. The morphology of spheroids is shown in **Figure 8**. The size of spheroids was about 400 µm at the first day. After 7 days, the spheroids incubated with BSA nanoparticles showed an obvious inhibition to the cell proliferation. It was observed that the entire spheroid structures had been destroyed with only small cores of residual cells remaining. At the same time the sizes of the LNCaP spheroids in the other two treatment groups (cell growth media only or a solution of 150 µM curcumin without carrier) swelled to more than 500 µm. These results were quantified by analyzing the amount of DNA in each sample (**Figure 9)**. It should be noted here that at these high concentrations both polymer-protein conjugates lead to similar results highlighting that both are toxic and efficient bullets at high enough drug concentration.

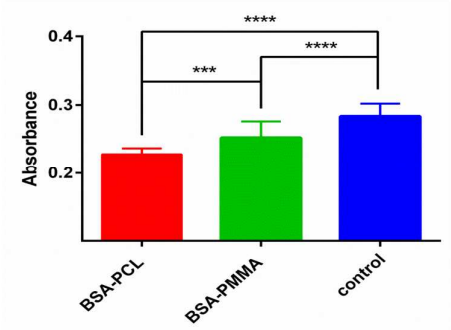

Figure 7. Prostate carcinoma LNCaP spheroids were treated with curcumin loaded BSA-PCL nanoparticles and BSA-PMMA nanoparticles for 7 days. Water was used as a control. The DNA amount in each group was checked. The higher absorbance indicates less cell death in the spheroid. The concentration of curcumin is 30 µM. Data are expressed as mean ± standard error, n=18. ***, statistical difference, p<0.001. ****, statistical difference, p<0.0001.

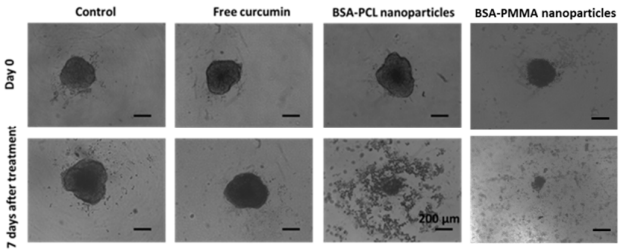

Figure 8. Prostate carcinoma LNCaP spheroids were treated with free curcumin and curcumin loaded BSA nanoparticles for 7 days. Water was used as a control. Scale bar is 200 µm.

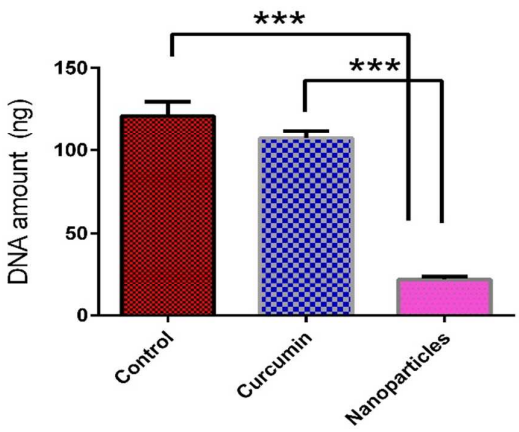

Figure 9. DNA amount in each group of each spheroid. The concentration of curcumin is 0.15 mM. Data are expressed as mean±standard error, n=3. ***, statistical difference, p<0.001.

Conclusions

In this study, curcumin loaded BSA-PCL nanoparticles were fabricated based on conjugating the resorbable PCL via Michael addition to BSA. In addition, a control sample based on PMMA and albumin was prepared. Both polymer-protein conjugates lead to spherical nanoparticles with similar curcumin loading efficiencies and release rates in buffer solution. These drug loaded carriers could be stored for an extended period of time as powder, while reconstitution in buffer solution was found to be quick with good recovery of the original particles. The cellular uptake was unaffected by the type of polymer with caveolae-mediated endocytosis dominating the uptake as expected for gp60 mediated albumin uptake. Also the toxicity of curcumin delivered in either nanoparticle was similar while the PMMA-based nanoparticles

were found to display faster movements in LNCaP spheroids. However, the PCL-based nanoparticles were shown to be more efficient in inhibiting the growth of the LNCaP spheroids due to its biodegradability. In conclusion, apart from the obvious advantages of resorbable polymers such as the potential absence of long-term accumulation in the body, the BSA-PCL nanoparticles were found to be more effective in delivering curcumin due to a dependable penetration into the LNCaP spheroids at a rate that allows sufficient release of the drug.

Acknowledgements

The authors like to thank the Australian Research Council (ARC DP140100240) for funding. A.D. acknowledges for the financial support from The Scientific & Technological Research Council of Turkey (TUBITAK) (Project No: 1059B191200208).

Notes and references

1. H. P. Ammon and M. A. Wahl, *Planta Med*, 1991, **57**, 1-7.
2. L. Li, F. S. Braiteh and R. Kurzrock, *Cancer*, 2005, **104**, 1322-1331.
3. M. L. Kuo, T. S. Huang and J. K. Lin, *Biochim Biophys Acta*, 1996, **1317**, 95-100.
4. K. Piwocka, K. Zablocki, M. R. Wieckowski, J. Skierski, I. Feiga, J. Szopa, N. Drela, L. Wojtczak and E. Sikora, *Exp Cell Res*, 1999, **249**, 299-307.
5. M. T. Huang, T. Lysz, T. Ferraro, T. F. Abidi, J. D. Laskin and A. H. Conney, *Cancer Res*, 1991, **51**, 813-819.
6. S. E. Chuang, M. L. Kuo, C. H. Hsu, C. R. Chen, J. K. Lin, G. M. Lai, C. Y. Hsieh and A. L. Cheng, *Carcinogenesis*, 2000, **21**, 331-335.
7. D. Ranjan, T. D. Johnston, K. S. Reddy, G. Wu, S. Bondada and C. Chen, *J Surg Res*, 1999, **87**, 1-5.
8. S. Lev-Ari, L. Strier, D. Kazanov, L. Madar-Shapiro, H. Dvory-Sobol, I. Pinchuk, B. Marian, D. Lichtenberg and N. Arber, *Clin Cancer Res*, 2005, **11**, 6738-6744.
9. A. Mukerjee and J. K. Vishwanatha, *Anticancer Res*, 2009, **29**, 3867-3875.
10. D. Giri, M. Ozen and M. Ittmann, *Am. J. Pathology*, 2001, **159**, 2159-2165.
11. R. A. Eeles, Z. Kote-Jarai, G. G. Giles, A. A. A. Olama, M. Guy, S. K. Jugurnauth, S. Mulholland, D. A. Leongamornlert, S. M. Edwards, J. Morrison, H. I. Field, M. C. Southey, G. Severi, J. L. Donovan, F. C. Hamdy, D. P. Dearnaley, K. R. Muir, C. Smith, M. Bagnato, A. T. Ardern-Jones, A. L. Hall, L. T. O'Brien, B. N. Gehr-Swain, R. A. Wilkinson, A. Cox, S. Lewis, P. M. Brown, S. G. Jhavar, M. Tymrakiewicz, A. Lophatananon, S. L. Bryant, A. Horwich, R. A. Huddart, V. S. Khoo, C. C. Parker, C. J. Woodhouse, A. Thompson, T. Christmas, C. Ogden, C. Fisher, C. Jamieson, C. S. Cooper, D. R. English, J. L. Hopper, D. E. Neal and D. F. Easton, *Nat Genet*, 2008, **40**, 316-321.
12. R. Jin, J. A. Sterling, J. R. Edwards, D. J. DeGraff, C. Lee, S. I. Park and R. J. Matusik, *PLoS ONE*, 2013, **8**, e60983.
13. J. Suh, F. Payvandi, L. C. Edelstein, P. S. Amenta, W. X. Zong, C. Gelinas and A. B. Rabson, *Prostate*, 2002, **52**, 183-200.
14. M. Saad, O. B. Garbuzenko and T. Minko, *Nanomedicine*, 2008, **3**, 761-776.
15. C. Yang, H. Chen, J. Zhao, X. Pang, Y. Xi and G. Zhai, *Colloids and Surfaces B: Biointerfaces*, 2014, **121**, 206-213.
16. G. Gaucher, M.-H. Dufresne, V. P. Sant, N. Kang, D. Maysinger and J.-C. Leroux, *Journal of Controlled Release*, 2005, **109**, 169-188.
17. W. Wu, Q. Zhang, J. Wang, M. Chen, S. Li, Z. Lin and J. Li, *Polym. Chem.*, 2014, **5**, 5668-5679.
18. W. Wu, J. Wang, Z. Lin, X. Li and J. Li, *Macromol. Rapid Commun.*, 2014, **35**, 1679-1684.
19. A. J. Dirks, R. J. M. Nolte and J. J. L. M. Cornelissen, *Advanced Mater.*, 2008, **20**, 3953-3957.
20. E. Garanger and S. Lecommandoux, *Angew. Chem. Inter. Ed.*, 2012, **51**, 3060-3062.
21. H.-N. Kim, J. Lee, H.-Y. Kim and Y.-R. Kim, *Chem. Commun.*, 2009, 7104-7106.
22. H. Y. Cho, M. A. Kadir, B.-S. Kim, H. S. Han, S. Nagasundarapandian, Y.-R. Kim, S. B. Ko, S.-G. Lee and H.-j. Paik, *Macromolecules*, 2011, **44**, 4672-4680.
23. S. L. Kuan, Y. Wu and T. Weil, *Macromol. Rapid Commun.*, 2013, **34**, 380-392.
24. B. Elsadek and F. Kratz, *J. Controlled Release*, 2012, **157**, 4-28.
25. D. Garmann, A. Warnecke, G. V. Kalayda, F. Kratz and U. Jaehde, *J. Controlled Release*, 2008, **131**, 100-106.
26. F. Kratz, *J. Controlled Release*, 2008, **132**, 171-183.
27. J. Ge, E. Neofytou, J. Lei, R. E. Beygui and R. N. Zare, *Small*, 2012, **8**, 3573-3578.
28. B. Le Droumaguet and K. Velonia, *Angewandte Chem. Inter. Ed.*, 2008, **47**, 6263-6266.
29. D. Garmann, A. Warnecke, G. V. Kalayda, F. Kratz and U. Jaehde, *J Controlled Release*, 2008, **131**, 100-106.
30. Y. Wu, G. Pramanik, K. Eisele and T. Weil, *Biomacromolecules*, 2012, **13**, 1890-1898.
31. Y. Jiang, R. Liang, D. Svejkar, H. Lu, G. Hart-Smith, W. Scarano and M. H. Stenzel, *Chem. Commun.*, 2014, **50**, 6394-6397.
32. T. Etrych, J. Strohalm, P. Chytil, P. Cernoch, L. Starovoytova, M. Pechar and K. Ulbrich, *Eur J Pharm Sci*, 2011, **42**, 527-539.
33. K. L. Heredia and H. D. Maynard, *Org. Biomol. Chem.*, 2007, **5**, 45-53.
34. S. Agarwal, Y. Zhang, S. Maji and A. Greiner, *Materials Today*, 2012, **15**, 388-393.
35. Y. Jiang, H. Lu, Y. Y. Khine, A. Dag and M. H. Stenzel, *Biomacromolecules*, 2014, **15**, 4195-4205.
36. Z. Liu, C. Dong, X. Wang, H. Wang, W. Li, J. Tan and J. Chang, *ACS Appl. Mater. Interfaces*, 2014, **6**, 2393-2400.
37. Y. Jiang, C. K. Wong and M. H. Stenzel, *Macromol. Biosci.*, 2015, **15**, 965-978.

38. A. P. Bapat, D. Roy, J. G. Ray, D. A. Savin and B. S. Sumerlin, *J Am Chem Soc*, 2011, **133**, 19832-19838.
39. T. Lammers, P. Peschke, R. Kühnlein, V. Subr, K. Ulbrich, J. Debus, P. Huber, W. Hennink and G. Storm, *J. Controlled Release*, 2007, **117**, 333-341.
40. G. Pan, Y. Zhang, Y. Ma, C. Li and H. Zhang, *Angew Chem Int Ed* 2011, **50**, 11731-11734.
41. T. Ramanathan, A. A. Abdala, S. Stankovich, D. A. Dikin, M. Herrera-Alonso, R. D. Piner, D. H. Adamson, H. C. Schniepp, X. Chen, R. S. Ruoff, S. T. Nguyen, I. A. Aksay, R. K. Prud'Homme and L. C. Brinson, *Nat Nanotechnol*, 2008, **3**, 327-331.
42. A. Jithan, K. Madhavi, M. Madhavi and K. Prabhakar, *Int J Pharm Investig*, 2011, **1**, 119-125.
43. M. A. Woodruff and D. W. Hutmacher, *Progr. Polym. Sci.*, 2010, **35**, 1217-1256.
44. K. M. Huh, S. C. Lee, Y. W. Cho, J. Lee, J. H. Jeong and K. Park, *J. Controlled Release*, 2005, **101**, 59-68.
45. W. Wang, *Int. J. Pharm.*, 2000, **203**, 1-60.
46. C. Tiruppathi, W. Song, M. Bergenfeldt, P. Sass and A. B. Malik, *J Biol Chem*, 1997, **272**, 25968-25975.
47. A. M. Merlot, D. S. Kalinowski and D. R. Richardson, *Front Physiol*, 2014, **5**, 299.
48. S. Oddi, F. Fezza, N. Pasquariello, A. D'Agostino, G. Catanzaro, C. De Simone, C. Rapino, A. Finazzi-Agrò and M. Maccarrone, *Chemistry & Biology*, 2009, **16**, 624-632.
49. Y. Kim, M. H. Pourgholami, D. L. Morris, H. Lu and M. H. Stenzel, *Biomater Sci*, 2013, **1**, 265-275.
50. H. Hillaireau and P. Couvreur, *Cellular and Molecular Life Sciences*, 2009, **66**, 2873-2896.
51. Y. Yan, G. K. Such, A. P. R. Johnston, J. P. Best and F. Caruso, *ACS Nano*, 2012, **6**, 3663-3669.
52. I. R. Nabi and P. U. Le, *The Journal of Cell Biology*, 2003, **161**, 673-677.
53. P. Anand, H. B. Nair, B. Sung, A. B. Kunnumakkara, V. R. Yadav, R. R. Tekmal and B. B. Aggarwal, *Biochemical Pharmacology*, 2010, **79**, 330-338.
54. N. R. Patel, B. S. Pattni, A. H. Abouzeid and V. P. Torchilin, *Adv. Drug Delivery Rev.*, 2013, **65**, 1748-1762.
55. H. Lu, R. H. Utama, U. Kitiyotsawat, K. Babiuch, Y. Jiang and M. H. Stenzel, *Biomater Sci*, 2015.
56. A. W. Du, H. Lu and M. H. Stenzel, *Biomacromolecules*, 2015, **16**, 1470-1479.

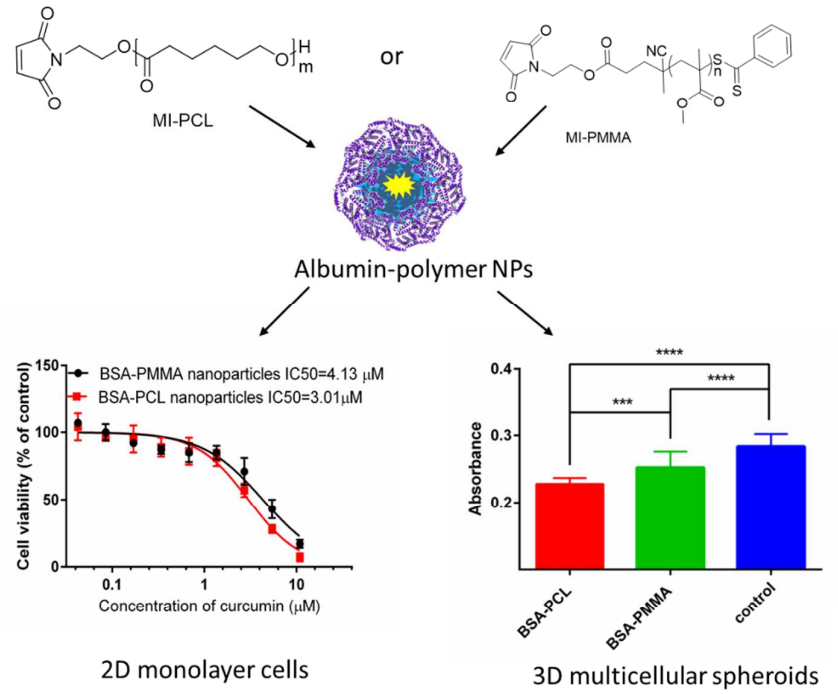
MI-PCL
or
MI-PMMA
Albumin-polymer NPs
BSA-PMMA nanoparticles IC50=4.13 μM
BSA-PCL nanoparticles IC50=3.01μM
Cell viability (% of control)
Concentration of curcumin (μM)
2D monolayer cells
Absorbance
BSA-PCL
BSA-PMMA
control
3D multicellular spheroids